Journal of Hazardous Materials 179 (2010) 1007–1013
doi:10.1016/j.jhazmat.2010.03.105

Utilization of activated CO_2-neutralized red mud for removal of arsenate from aqueous solutions

Ramesh Chandra Sahu [a], Rajkishore Patel [a], Bankim Chandra Ray [b]

[a] *Department of Chemistry,* [b] *Department of Metallurgical and Materials Engineering*

[a, b] *National Institute of Technology, Rourkela 769008, Orissa, India*

E-mail address: rcsahu.chem@gmail.com

Abstract

A laboratory study was conducted to investigate the ability of activated CO_2-neutralized red mud (ANRM) for the removal of arsenate from the aqueous solutions. The batch adsorption experiments were conducted with respect to adsorbent dose, equilibrium pH, contact time, initial arsenate concentration, kinetics, Langmuir isotherms. The mechanisms involved in adsorption of arsenate ions on ANRM were characterized by using XRD, FT-IR, UV–vis, SEM/EDX, and chemical methods. The percentage removal was found to increase gradually with decrease of pH and maximum removal was achieved at pH ~4. Adsorption kinetic studies revealed that the adsorption process followed pseudo-second-order kinetics and equilibrates within 24 h. FT-IR spectra of ANRM before and after adsorption reveals the binding of arsenate to the adsorbent. The adsorption data were fitted to linearly transformed Langmuir isotherm with R^2 (correlation coefficient) > 0.99. Arsenate adsorbed ANRM can be regenerated using NaOH solution at pH 12.0.

Keywords: Red mud; CO_2; Arsenate; Kinetics; Isotherms

1. Introduction

Arsenic contaminated water is one of the most challenging global environmental problems today. Millions of people worldwide are exposed to this water as their only source of drinking water, due to natural and man-made sources. Arsenic can be easily solubilized in ground waters depending on pH, redox conditions, temperature, and solution composition [1]. Long-term exposure to arsenic contaminated water causes various types of cancers. Therefore, World Health Organization (WHO) has recommended the standard concentration of arsenic in drinking water is 10 μg L^{-1} [2]. But the typical arsenic concentration in arsenic contaminated water used for human consumption is about 100–300 μg L^{-1} [3].

Various methods for arsenate removal have been investigated for the rising demand of standard drinking water. Thus, there is growing interest for development of low-cost materials and methods to remove arsenic from drinking water or industrial effluents before it may cause significant contamination. Although many different methods such as precipitation, coprecipitation of aluminum and iron hydroxides [4,5], adsorbing colloid flotation, ion-exchange, ultrafiltration, and reverse osmosis has been used for arsenic removal [6], but the process based on adsorption methods are promising, due to high concentration removal efficiency. Many types of adsorbents have been used: goethite [7], iron oxide minerals [8], zerovalent iron [9], soil [10,11], high surface area iron oxide based sorbent [12], activated red mud[13], Bauxsol and activated Bauxsol [14, 15], are mostly used in arsenic adsorption, due to strong affinity of iron toward arsenic. Arsenic is mostly present in the form of arsenate [As(V)] and arsenite [As(III)] in natural water. Both As(V) and As(III) sorbs more efficiently to iron oxides [8].

Previous research has observed strong adsorption of arsenic to seawater neutralized RM (Bauxsol), further activated by acid treatment or combined acid and heat treatment method [14, 15]. The results showed that combination of acid and heat treatment has greater removal efficiency.

Red mud (RM) is a waste product formed after caustic digestion of bauxite during the extraction of alumina. The storage and maintenance of red mud is a challenging environmental problem in the alumina industry area due to its alkaline nature, which is a risk for living organisms. It also pollutes the ground water and air borne dust impact on industry [16–19]. Furthermore, arsenate adsorption mainly takes place in acidic medium [15,20]. So, its neutralization using CO_2 sequestration and utilization for environmental benefit enhance the socio-ecological-economical value of alumina industries.

With our knowledge from literature survey, the removal of arsenate from aqueous solutions using activated CO_2–neutralized red mud has not been reported. The objective of this study is to characterize the arsenate adsorption on the ANRM and to investigate the removal of arsenate from the aqueous solutions by batch experiments. The effect of various parameters, adsorbent dose, time, pH, effect of initial arsenate concentration, etc. on the removal of arsenate from aqueous solutions by ANRM was examined. The ultimate aim is also to try to find out the optimum conditions of reuse of ANRM as a low-cost sorbent.

2. Materials and methods

2.1. Materials

All chemicals, including HCl, NaOH, HNO_3, $NaBH_4$, KI, KBr and arsenic standard solution of 1000 mg L^{-1} used in the present study were of analytical grade and obtained from Merck (Germany), sodium arsenate heptahydrate ($Na_2HAsO_4.7H_2O$), NaCl from Nice chemicals and L–

cysteine from Loba chemicals, $BaSO_4$ from Wako pure chemicals. In all experiments, double distilled water was used for preparation, dilution and analytical purposes of the solutions. As(V) stock solution of 1000 mg L^{-1} was prepared by dissolving 4.164 g $Na_2HAsO_4.7H_2O$ in 1 L of double distilled water. Test solutions of arsenate with concentrations 7–100 mg L^{-1} were prepared from the stock solution.

2.2. Adsorbent preparation

The fresh red mud used in this study was obtained from R&D Laboratory of NALCO, Damanjodi, Orissa, India, in the form of dried-clay. The chemical compositions of the RM based on the dry weight are Fe_2O_3 (54%), Al_2O_3 (13%), SiO_2 (7%), Na_2O (8%), and TiO_2 (3.5%). The RM was neutralized using sequestration of CO_2 gas. The pH of RM suspension was decreased from 11.8 to 8.45. This partially neutralized RM sample was dried at 110 °C for 2 h and calcinated at 500 °C for 2 h and referred as activated neutralized red mud (ANRM).

2.3. Characterization of adsorbent

The powder X-ray diffraction (XRD) of sample was determined by using Philips X'Pert X-ray diffractometer with a Cu Kα radiations generated at 35 kV and 30 mA. Scattering angle 2θ was ranged from 10–80º at a scanning rate of 2 º min^{-1} and was analyzed using standard software provided with the instrument. The surface micro-morphology of materials was investigated using a Scanning Electron Microscope (SEM) and qualitative element composition was analyzed using Energy Dispersive X-ray (EDX) by JOEL model JSM-6480LV (Japan).

The BET surface area was measured at liquid nitrogen temperature using the Brunauer–Emmett–Teller (BET) surface area analyzer (Quantachrome AUTOSORB–1, USA). All samples were degassed at 150 °C in vacuum. Helium was used as carrier gas and surface area was measured by nitrogen adsorption–desorption method. Particle size of the red mud was measured

using Master Sizer (Malverns, UK). FT-IR spectra of the samples were obtained by using PerkinElmer FT-IR Spectrometer Spectrum RX-I. The spectrum was scanned from 4000 to 400 cm^{-1}. Samples were homogeneously crushed with anhydrous KBr in a ratio of 1:50. The powder was pressed at 10 tons cm^{-2} to make a translucent tablet for recording FTIR spectra. The diffuse reflectance spectra of powder samples were carried out on a UV–vis spectrophotometer (UV–2450; Shimadzu, Japan) at room temperature and $BaSO_4$ was used as a reflectance standard.

The pH measurements of arsenate aqueous solutions were made using a calibrated Orion 2 Star Bench top pH meter. Quantitative analysis of the As(V) ion in the filtrate, after adsorption was determined by using hydride generated atomic absorption spectrometer (MHS 15, AAS, PerkinElmer, AAnalyst 200, U.S.A.) using standard method. Calibration was achieved using dilutions prepared from a commercially available 1000 mg L^{-1} standard arsenic solution [21,22]. For hydride generation, 3% $NaBH_4$ (prepared in 1% NaOH) and 1.5% HCl solutions were reacted with the samples for total As determination.

2.4. Batch experiments:

Batch experiments were carried out at room temperature (25 ± 2 ºC) using 100 mL stoppered polylab plastic bottles. 0.2 g of ANRM adsorbent was weighted and put into the different plastic bottles, into which 50 mL of As(V) solutions at initial concentration 1–100 mg L^{-1} were added separately. The bottles were capped tightly for all tests to avoid change in concentration, due to evaporation. The pH was adjusted to the desired level with 0.1 M NaOH or 0.1 M HCl solutions. A number of experimental parameters such as adsorbent dose, contact time, initial arsenate concentration, pH affecting the adsorption of arsenate have been studied to optimize the removal process. The solutions were stirred using magnetic stirrer at about 300 rpm for 24 h until the adsorption equilibrium time was reached. All adsorption studies were carried out at a constant

ionic strength of 0.01 M maintained with NaCl. After stirring, the solutions were allowed to settle for 10 min and the samples were centrifuged 3000 rpm for 20 min and filtered through Whatman 42 filter paper. The filtrate was used for the analysis of remaining arsenate concentration in the solution. The amount of arsenate adsorbed (removal) was calculated as follows:

$$\%adsorbed = \frac{[C]_i - [C]_f}{[C]_i} \times 100 \quad (1)$$

where $[C]_i$ and $[C]_f$ are the initial and final concentrations of the arsenate in the aqueous solutions (mg L^{-1}), respectively. All experiments were conducted in duplicate and the mean values were considered.

2.5. Desorption and regeneration studies

The recovery of the adsorbed As(V) ions as well as reusability of activated red mud mainly depends on the ease with which arsenate (V) ions get desorbed from loaded ANRM sample. For this 50 mL of 10 mg L^{-1} arsenate solution was treated with 0.2 g of ANRM and was kept under stirring for 24 h. The content of the flask was filtered and separated. The filtered adsorbent was retreated with 50 mL neutral distilled water and they were adjusted to different pH with the help of 1.0 M NaOH. The samples were stirred at 300 rpm at room temperature (25 ± 2 °C) for 24 h.

3. Results and discussion

3.1. Characterization of adsorbent

Particle size of the red mud was in the range of 0.1 – 160 μm. The BET-N_2 surface area of RM, NRM and ANRM were found to be 31.7, 59.33 and 63 m^2 g^{-1}, respectively. The surface areas of NRM and ANRM were increased, due to acidic CO_2 and thermal treatment, respectively.

The crystalline phases of RM, NRM and ANRM were obtained by powder XRD and the graph is presented in Fig. 1. The following mineral phases were analyzed with Philips X'Pert High Score software: hematite (α-Fe_2O_3), goethite (α-FeO(OH)), gibbsite (γ-$Al(OH)_3$), calcite ($CaCO_3$), rutile/anatase (TiO_2), sodalite: zeolite (I) ($1.08Na_2OAl_2O_31.68SiO_21.8H_2O$), quartz ($SiO_2$), sodium aluminum silicate ($Na(AlSiO_4)$), and magnetite (Fe_3O_4). The results obtained from the analysis indicated that there were remarkable differences among RM, NRM, and ANRM, which suggests that phase transformation has taken place. It revealed that the peaks of gibbsite in NRM were increased prominently and a new mineral ilmenite ($FeTiO_3$) was formed, due to CO_2 treatment. But, after thermal treatment of NRM, the intensity of hematite was increased significantly, whereas the peaks of gibbsite disappeared, due to decomposition. As a result, hematites are dominant phases in ANRM.

Fig. 2 shows the FT-IR spectra of RM, NRM and ANRM. The positions of the absorption bands are nearly similar in all spectra. But, the relative intensities of RM are more intense. RM showed a broad band at ~3142 and a weak peak at ~1644 cm^{-1}, due to the stretching vibrations of O–H bonds and H–O–H bending vibrations of interlayer adsorbed H_2O molecule respectively. Water hydroxyl-stretching vibrations are intense in an infrared spectrum, because of large change in dipole moment. The OH-stretching vibrations of NRM and ANRM show at higher wave number of ~3461, 3396 cm^{-1}, respectively. This shift is associated with the shorter O–H bonds existing in RM than NRM and ANRM, causing an increase in electrostatic attraction within the RM layer. The absorption bands at ~1473, ~1410 and ~807 of RM and ~1486, ~1410 and ~803 cm^{-1} of NRM are due to stretching vibrations of C=O, confirmed the presence of CO_3^{2-} groups [23–25]. This may be due to chemisorbed CO_2 in RM and NRM, respectively. These peaks were disappeared in ANRM, due to decomposition of carbonate group by heat

treatment. Characteristic bands correspond to Si–O vibration were detected at ~993 – ~1007 cm^{-1} proved the presence of silicate groups. Peaks at ~553 – ~546 and ~469 – ~459 cm^{-1} are due to bending vibration of Si–O–Al and stretching vibrations of Fe–O bonds, respectively [19,26]. Intensities of these peaks were decreased in NRM, ANRM which confirmed the dissolution of minerals like silicate, $Na(AlSiO_4)$. Hence, FT-IR results support the evidence of phase change data of XRD.

The diffuse reflectance spectra of powder samples were converted into the absorption spectra by the Kubelka–Munk relationship, $K/S = (1 - R)^2/2R$, where R, K, and S are the value of reflectance measurements (relative value to the reflectance of $BaSO_4$) and the absorption and scattering coefficients of the sample, respectively. Fig. 3 shows the UV–vis diffuse reflectance and absorption spectra of RM, NRM and ANRM. It shows that the peak maxima are observed at slightly different positions for the three samples and the spectral patterns are very similar. However, the absorbance peak broadening of ANRM was observed, as shown Figure 3 (inset). This study of spectra suggests that there is no effect of CO_2-neutralization and further heat treatment on the structure of Fe^{3+} ions of Fe_2O_3. In the region from 600 – 800 nm UV-vis light was not absorbed, which determines the red color from Fe^{3+} of RM, NRM and ANRM. As a result, in this region maximum reflection of light radiation was observed. Furthermore, reflectance % and peaks broadening of solid powder samples gradually decreased depending upon the decrease of concentration of alkaline oxides.

SEM micrograph (Fig. 4) provides the surface micro morphology of the ANRM. Some mineral phase mainly calcite, sodalite, quartz were soluble in acidic environment. As a result their rounded shapes of aggregate disappeared. On thermal treatment porosity of the material was developed. The EDX spectra of ANRM shows the presence of Fe, O, Al, Ti, Si and C.

3.2. Effect of adsorbent dose and pH

It is evident from the Fig. 5 that the % removal of As(V) was increased from ~73 – ~98% with increase of the adsorbent concentration (1–4 g L^{-1}) with initial arsenate concentration of 10 mg L^{-1}. Because number of active sites increases with respect to increase of adsorbent dose. However, it was observed that after dose of 4 g L^{-1}, there was no significant change in % removal of As(V). This may be due to overlapping of active sites at higher dose. So, there was not any appreciable increase in the effective surface area due to the agglomeration of exchanger particles [27]. So, 0.2 g/50 mL was considered as optimum dose and was used for further study. Some experiments were carried out to examine the effect of initial pH on the adsorption. The arsenate removal was favored at acidic pH (3–6), whereas adsorption gradually decreased with increase of pH. Furthermore, the adsorption of As(V) was very low at pH 10.0, as shown in Fig. 6.

Solution pH not only affects the surface charge property of the ANRM through the protonation, but also influences arsenate speciation in the solution. Arsenate exists as H_3AsO_4, $H_2AsO_4^-$, $HAsO_4^{2-}$, and AsO_4^{3-} species in aqueous solution. $H_2AsO_4^-$ is the main species in solution at pH from 3–6, while $HAsO_4^{2-}$, and AsO_4^{3-} become major species at pH above 8. Therefore, arsenate species are anionic in this pH range. With increase of solution pH, the number of protonated groups (positive charges) on ANRM decreased, while the number of negative charge of arsenic species increased. As a consequence, the adsorption amount of ANRM for arsenate decreased. In acidic environment, OH^- ions concentration in the solution is lower, so less competition with As(V) anions for the available active sites. The above data suggest that the optimum pH for removal of arsenate was ~4. In the pH range 3–7, $H_2AsO_4^-$ and $HAsO_4^{2-}$ are the predominant species of As. Solutes interact with mineral surfaces due to their

electrical surface charge, because of reactions involving functional groups (H^+, OH^-) on the mineral surface and ions in the solution. Hydroxylated surface of the oxides of red mud develops charge on the surface in the water. The adsorption between surface hydrohyl group and As(V) ion follows ligand exchange reaction mechanism and exists as inner sphere surface complexes [15]. The binuclear bidentate surface complex $\equiv(FeO)_2AsO_2^-$ is predominated and the dominant form of arsenate in the range of pH 4–6.8, whereas the monodentate complex $\equiv FeOAsO_3^{2-}$ is dominate above pH 6.8 [12]. This involves columbic interaction and is referred as surface coordination:

$$\equiv S–OH + L^- + H^+ \leftrightarrow \equiv S–L + H_2O \quad (2)$$

where ≡S–OH is a surface hydroxyl group and ≡S–L is the ligand-adsorbed species. Red mud is a heterogeneous mixture of several minerals. The hydroxyl surfaces of mixture of Fe, Al, Ti oxides of ANRM provide strong adsorption affinity for arsenate adsorption by forming inner-sphere complexes.

The adsorbed As(V) on ferric hydroxide shows two peaks at 835 and 938 cm^{-1} in acidic medium as shown in Fig. 7. This is due to symmetric stretching (ν_s) of As–O bond and asymmetric stretching (ν_{as}) of As–O bond in As–O–Fe species, respectively. The peak position is strongly affected by changes in pH. Therefore, they show prominent peaks at optimum acidic pH. From FT-IR data there is a clear evidence for surface precipitation of poorly crystalline ferric arsenate in acidic pH ~4, whereas at alkaline pH arsenate is adsorbed via surface complexation. The observed As(V) FT-IR bands at various pH are in agreement with previous reports [28–32].

3.3. Effect of contact time and adsorption kinetics

Adsorption of As(V) at different contact time was studied for determination of equilibrium time of reaction. These experiments were carried out at equilibrium pH ~4, with initial arsenate concentration 10 mg L^{-1} at room temperature. The percentage removal was 85% for first 0.5 h of contact time. The results of the Fig. 8 showed that the maximum removal was 99% and attained equilibrium at 24 h. After that there was no significant change in the percentage removal. This indicates the possible monolayer formation of As(V) ions on the outer surface.

The rate constant K_1 for adsorption of As(V) was studied by Lagergren rate equation [14] for initial arsenate concentration of 10 mg L^{-1}. Pseudo-first-order rate expression of Lagergren equation:

$$\log(q_e - q_t) = \log q_e - \frac{K_1 t}{2.303} \tag{3}$$

where q_e and q_t are the amount of arsenate adsorbed (mg g^{-1}) at equilibrium and at time t (min), respectively. K_1 is the pseudo-first-order rate constant (min^{-1}). The K_1 and R^2 were found to be 0.0076 and 0.939 respectively, which are extremely low, indicating that the adsorption of As(V) onto ANRM did not follow pseudo-first-order rate model.

The pseudo-second-order rate expression:

$$\frac{t}{q_t} = \frac{1}{K_2 q_e^2} + \frac{t}{q_e} \tag{4}$$

where K_2 is the pseudo-second-order rate constant (g mg^{-1} min^{-1}). The values of K_2, and R^2 were given in Table 1. The low value of K_2 and high value of R^2 indicates that the adsorptions followed pseudo-second-order kinetics.

3.4. Adsorption equilibrium isotherms

Commonly adsorption isotherm has been used to evaluate the adsorption capacity of an adsorbent for an adsorbate. The linearized Langmuir adsorption isotherm equation is as follows [33]:

$$\frac{1}{q_e} = \frac{1}{q_m b C_e} + \frac{1}{q_m} \quad (5)$$

where C_e is the equilibrium concentration of adsorbate in solution (mg L^{-1}), q_e is the amount adsorbate adsorbed at equilibrium (mg g^{-1}), q_m is the theoretical maximum adsorption capacity (mg g^{-1}), and b is the Langmuir constant (L mg^{-1}). Arsenate adsorption is well fitted by Langmuir adsorption isotherm with correlation coefficient R^2 = 0.996, as shown in Fig. 9. This indicates a monolayer sorption of arsenate onto the adsorbent surface. The maximum adsorption capacity (q_m) of ANRM for arsenate was 55.55 mg g^{-1} according to Langmuir model, which is better than that of most adsorbents [13–16], single component materials [34] used to remove arsenate in the literature.

Freundlich adsorption isotherm assumes multilayer adsorption on heterogeneous surfaces. Linearized form of the Freundlich equation is given by the following equation [14]:

$$\ln q_e = \ln K_f + 1/n \ln C_e \quad (6)$$

where q_e is the amount of arsenate ions adsorbed at equilibrium time (mg g^{-1}), C_e is the equilibrium concentration of arsenate ions in the solution (mg L^{-1}), K_f is the adsorption capacity (mg g^{-1}), and n is an empirical parameter. The value of K_f, n, *and* R^2 are 10.86 mg g^{-1}, 2.0411, 0.977, respectively. This indicates that the highest correlation coefficient of Langmuir isotherm fits the adsorption data better than the Freundlich isotherm.

3.5. Desorption and regeneration studies

Regeneration studies were carried out in order to know the reusability of ANRM, when the adsorption capacity of the adsorbent is exhausted. Initially, desorption of arsenate was difficult in the pH range 4–8. Because, in the pH range of 4–9, Lewis bases ligands arsenates get selectively adsorbed through the formation of inner-sphere complexes [35]. But, as the pH increases from 9–12, desorption of arsenate increases and maximum desorption (92%) occurred at pH 12, as shown in Fig. 10. Because, at pH > 11.0, negatively charged FeO^- is the predominant surface functional group, thus rejects all ions including arsenates [36]. Therefore, desorption of arsenate with NaOH solution is very efficient. The surface of adsorbent (ANRM) becomes fresh and active sites are regenerated. But, adsorption capacity of regenerated ANRM decreases gradually, chemisorptions exhibits poor desorption, adsorbate species are bound tightly to the adsorbent with comparatively stronger bonds [14].

4. Conclusions

Adsorption is one of the most commonly used cost effective techniques to remove arsenate from contaminated water. In this study, red mud was neutralized using CO_2 and thermally activated neutralized red mud was used as adsorbent. FT-IR analysis revealed that the adsorption of As(V) on the surface of ANRM through the electrostatic interaction between the positively protonated hydroxyl groups and negatively charged arsenate. The percentage removal was increased with decrease of pH and attained maximum adsorption at pH ~4. The adsorption kinetics was found to follow pseudo-second-order rate law and equilibrates within 24 h. The ANRM can be used as a low cost adsorbent for the removal of arsenate to meet its acceptable

limit in water. This process can be employed as a preliminary investigation for utilization of ANRM for removal of arsenate from aqueous solutions.

Acknowledgements

The authors would like to thank "Council of Scientific and Industrial Research (CSIR), New Delhi, India)" for financial support. The authors also thank Prof. S. K. Sarangi, Director, NIT, Rourkela for providing necessary facilities and B. W. Herry (DGM, R&D, NALCO, Damanjodi, India) for providing fresh dried red mud.

References

[1] D.K. Nordstrom, Worldwide occurrences of arsenic in ground water, Science. 296 (21) (2002) 2143–2145.

[2] A.H. Smith, P.A. Lopipero, M.N. Bates, C.M. Steinmaus, Arsenic epidemiology and drinking water standards, Science. 296 (21) (2002) 2145–2146.

[3] M. Zaw, M.T. Emett, Arsenic removal from water using advanced oxidation process, Toxicology Letters. 133 (2002) 113–118.

[4] Y. Masue, R.H. Loeppert, T.A. Kramer, Arsenate and arsenite adsorption and desorption behavior on coprecipitated aluminum: iron hydroxides, Environ. Sci. Technol. 41 (2007) 837–842.

[5] X. Meng, S. Bang, G.P. Korfiatis, Effect of silicate, sulfate, and carbonate on arsenic removal by ferric chloride, Water Res**.** 34 **(**4**)** (2000) 1255–1261.

[6] J.A. Munoz, A. Gonzalo, M. Valiente, Arsenic adsorption by Fe(III)-loaded poen-celled cellulose sponge. Thermodynamic and selectivity aspects, Environ. Sci. Technol. 36 (2002) 3405-3411.

[7] J.S. Zhang, R. Stanforth, S.O. Pehkonen, Irreversible adsorption of methyl arsenic, arsenate, and phosphate onto goethite in arsenic and phosphate binary systems, J. Colloid Interface Sci. 317 (2008) 35–43.

[8] S. Dixit and J.G. Hering, Comparison of arsenic (V) and arsenic (III) sorption onto iron oxide minerals: implications for arsenic mobility, Environ. Sci. Technol. 37 (2003) 4142–4189.

[9] C. Su, R.W. Puls, Significance of iron(II, III) hydroxycarbonate green rust in arsenic remediation using zerovalent iron in laboratory column tests, Environ. Sci. Technol. 38 (2004) 5224–5231.

[10] H. Zhang, H.M. Selim, Kinetic of arsenate adsorption–desorption in soil, Environ. Sci. Technol. 39 (2005) 6101–6108.

[11] Z. Chen, Y. Cai, H.S. Gabriele, G.H. Snyder, J.L. Cisar, Interactions of arsenic and the dissolved substances derived from turf soils, Environ. Sci. Technol. 40 (2006) 4659–4665.

[12] H. Zeng, B. Fisher, D.E. Giammar, Individual and compettitive adsorption of arsenate and phosphate to a high-surface-area iron oxide-based sorbent, Environ. Sci. Technol. 42 (2008) 147–152.

[13] H.S. Altundogan, S. Altundogan, F. Tumen, M. Bildik, Arsenic adsorption from aqueous solutions by activated red mud, Waste Management. 22 (2002) 357–363.

[14] H. Genc-Fuhrman, J.C. Tjell, D. McConchie, Adsorption of arsenic from water using activated neutralized red mud, Environ. Sci. Technol. 38 **(**2004) 2428–2434.

[15] H. Genc-Fuhrman, J.C. Tjell, D. McConchie, Increasing the arsenate adsorption capacity of neutralized red mud (Baxsol), J. Colloid Interface Sci. 271 (2004) 313–320.

[16] C. Brunori, C. Cremisini, P. Massanisso, V. Pinto, L. Torricelli, Reuse of a treated red mud bauxite waste: studies on environmental compatibility, J. Hazard. Mater. B117 (2005) 55–63.

[17] C. Shi, J. Xu, E. Beckman, R. Enick, Carbon dioxide sequestration via pH reduction of red mud using liquid CO_2, ACS Division of Fuel Chem. 45(4) (2000) 703-705.

[18] W. Huang, S. Wang, Z. Zhu, L. Li, X. Yao, V. Rudolph, F. Haghseresht, Phosphate removal from water using red mud, J. Hazard. Mater. 158 (2008) 35–42.

[19] S.J. Palmer, R.L. Frost, T. Nguyen, Hydrotalcites and their role in coordination of anions in Bayer liquors: anion binding in layered double hydroxides, Coordi. Chem. Rev. 253 (2009) 250-267.

[20] W.R. Richmond, M. Loan, J. Morton, G.M. Parkinson, Arsenic removal from aqueous solution via ferrihydrite crystallization control, Environ. Sci. Technol. 38 **(**2004) 2368–2372.

[21] ASTM D 2972–03, Standard Test Methods for Arsenic in Water, Test Method B, 2007.

[22] A.E. Greenberg, R.R. Trussell, L.S. Clesceri, Standard Methods for the Examination of Water and Wastewater, 16th ed., APHA, AWWA, WPCF, Washington, DC, 2005.

[23] C. Cardell, I. Guerra, J. Romero-Pastor, G. Cultrone, A. Rodriguez-Navarro, Innovative analytical methodology combining micro-X-ray diffraction, scanning electron microscopy-based mineral maps, and diffuse reflectance infrared fourier transform spectroscopy to characterize archeological artifacts, Anal. Chem. 81(2) (2009) 604-611.

[24] P. Regnier, A.C. Lasaga, R.A. Berner, Mechanism of CO_3^{2-} substitution in carbonate-fluorapatite: evidence from FTIR spectroscopy, ^{13}C NMR, and quantum mechanical calculations, American mineralogist. 79 (1994), 809-818.

[25] R.V. Siriwardane, C. Robinson, M. Shen, T. Simonyi, Novel regenerable sodium-based sorbents for CO_2 capture at warm gas temperatures, Energy & Fuels. 21 (2007) 2088-2097.

[26] A. Gok, M. Omastova, J. Prokes, Synthesis and characterization of red mud/polyaniline composites: electrical properties and thermal stability, Eur. Polym. J. 43 (2007) 2471–2480.

[27] H. Tahir, Comparative trace metal contents in sediments and the removal of the chromium using Zeolite–5A, EJEAF Chem. 4(4) (2005) 1021–1032.

[28] C. Jing, G.P. Korfiatis, X. Meng, Immobilization mechanisms of arsenate in iron hydroxide sludge stabilized with cement, Environ. Sci. Technol. 37 (2003) 5050–5056.

[29] Y. Jia, L. Xu, Z. Fang, G.P. Emopoulos, Observation of surface precipitation of arsenate on ferrihydrite, Environ. Sci. Technol. 40 (2006) 3248–3253.

[30] A. Voegelin, S.J. Hug, Catalyzed oxidation of arsenic(III) by hydrogen peroxide on the surface of ferrihydrite: an in situ ATR-FTIR study, Environ. Sci. Technol. 37 (2003) 972–978.

[31] X.H. Guan, T. Su, J. Wang, Quantifying effects of pH and surface loading on arsenic adsorption on nanoactive alumina using a speciation-based model, J. Hazard. Mater. 166 (2009) 39–45.

[32] M. Pena, X. Meng, G.P. Korfiatis, C. Jing, Adsorption mechanism of arsenic on nanocrystalline titanium dioxide, Environ. Sci. Technol. 40 (2006) 1257–1262.

[33] L. Yang, S. Wu, J.P. Chen, Modification of activated carbon by polyaniline for enhanced adsorption of aqueous arsenate, Ind. Eng. Chem. Res. 46 (2007) 2133–2140.

[34] X.H. Guan, J. Wang, C.C. Chusuei, Removal of arsenic from water using granular ferric hydroxide: Macroscopic and microscopic studies, J. Hazard. Mater. 156 (2008) 178–185.

[35] S.R. Kanel, J.M. Greneche, H. Choi, Arsenic (V) removal from ground water using nano scale zero-valent iron as a colloidal reactive barrier material, Environ. Sci. Technol. 40 (2006) 2045–2050.

[36] L. Cumbal, A.K. Sengupta, Arsenic removal using polymer-supported hydrated iron (III) oxide nanoparticles: role of Donnan membrane effect, Environ. Sci. Technol. 39 (2005) 6508–6515.

List of Figures

Fig.1. XRD patterns of RM, NRM, and ANRM.

Fig.2. FT-IR patterns of RM, NRM, and ANRM.

Fig.3. UV–vis diffuse reflectance spectra of (1) RM, (2) NRM, and (3) ANRM. The inset is the enlarged view of the spectra between 285–390 nm.

Fig.4. SEM micrographs/EDX spectra of ANRM.

Fig.5. Adsorbent dose versus percentage removal of As(V) by ANRM.

Fig.6. Effect of initial pH on As(V) adsorption on ANRM.

Fig.7. FT-IR patterns of As(V) adsorbed on ANRM at different pH.

Fig.8. Time versus percentage removal of As(V).

Fig. 9. Langmuir adsorption isotherm plot of $1/C_e$ versus $1/q_e$.

Fig.10. Desorption of arsenate with respect to solution pH.

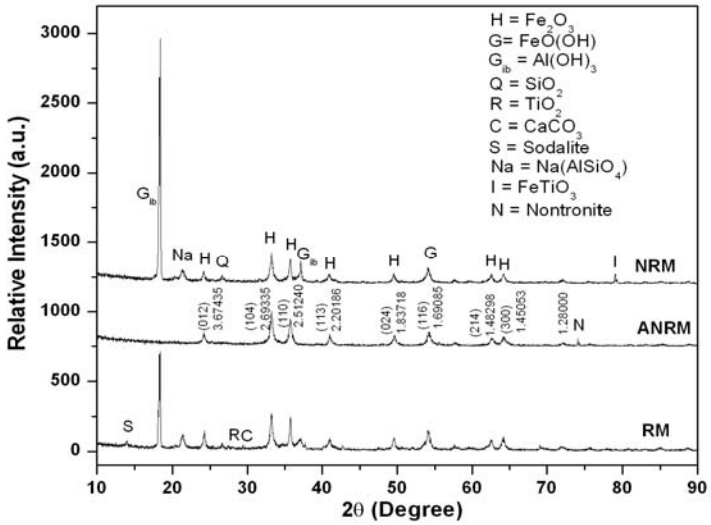

Fig.1.

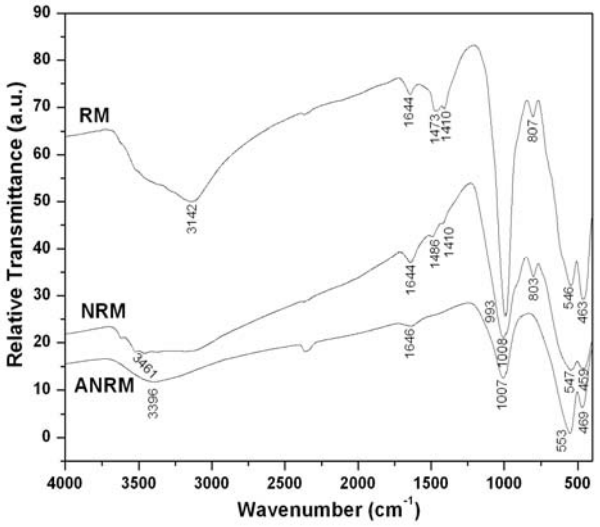
RM
NRM
ANRM
Relative Transmittance (a.u.)
Wavenumber (cm-1)
3142
1644
1473
1410
807
3461
3396
1646
1644
1486
1410
993
1008
1007
803
546
463
547
459
553
469

Fig.2.

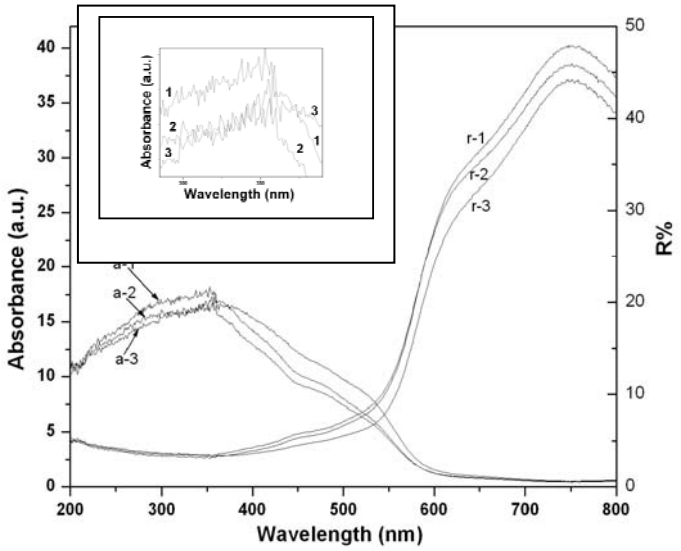
Absorbance (a.u.)
Wavelength (nm)
R%
a-1
a-2
a-3
r-1
r-2
r-3
1
2
3

Fig.3.

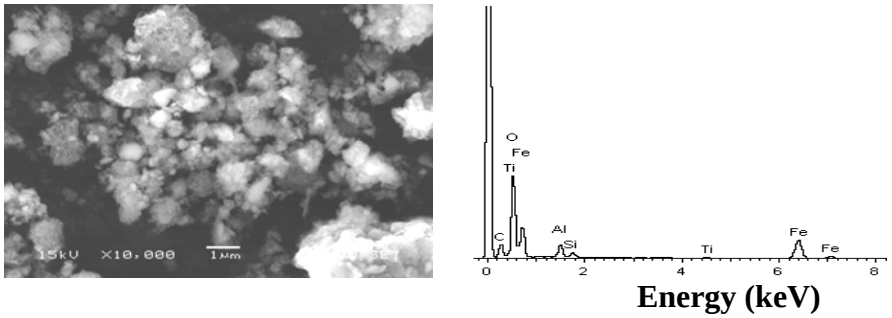

Fig.4.

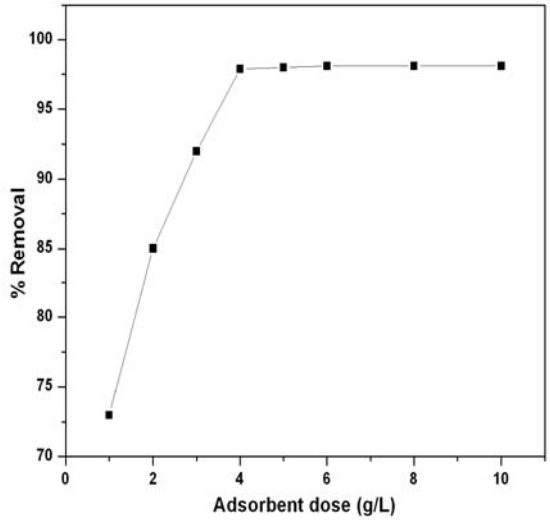

Fig.5.

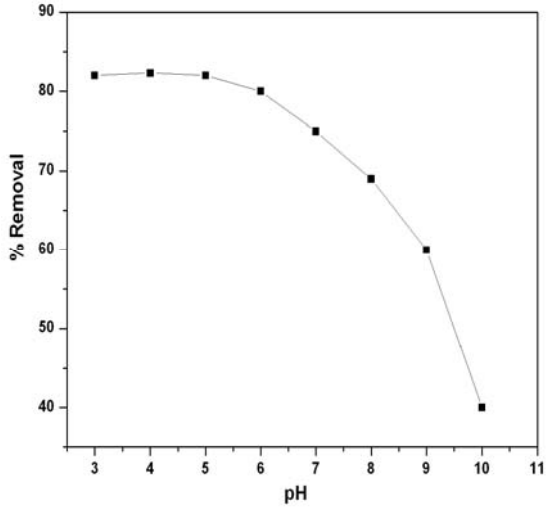

Fig.6.

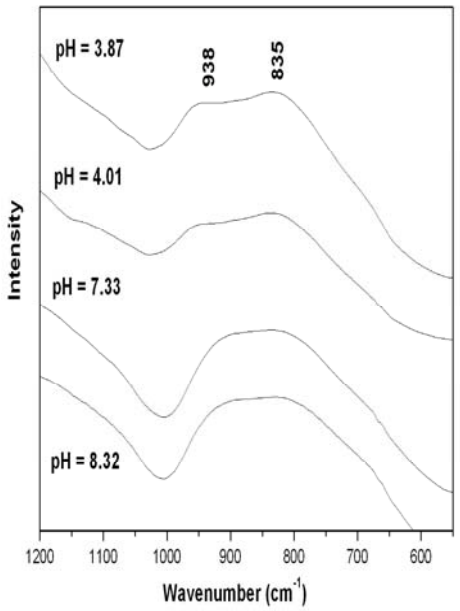
pH = 3.87
938
835
pH = 4.01
pH = 7.33
pH = 8.32
Intensity
1200
1100
1000
900
800
700
600
Wavenumber (cm-1)

Fig.7.

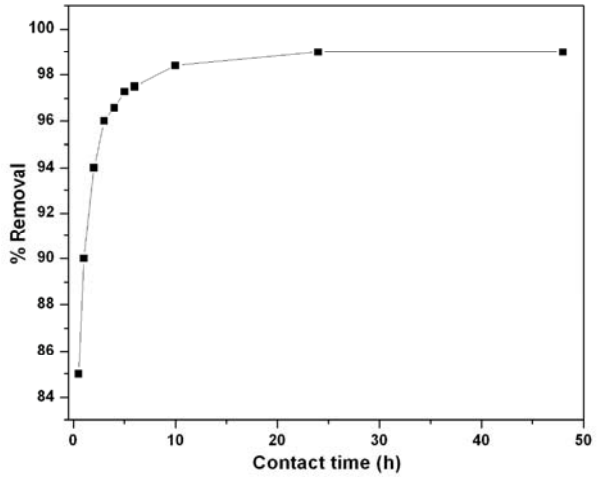
100
98
96
94
92
90
88
86
84
% Removal
0
10
20
30
40
50
Contact time (h)

Fig.8.

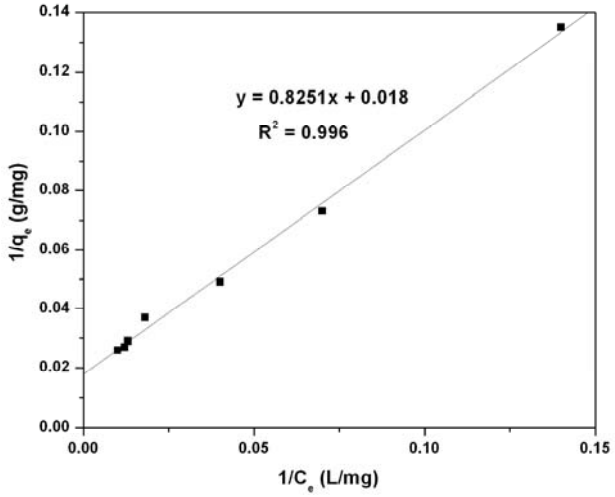
y = 0.8251x + 0.018
R² = 0.996
1/qe (g/mg)
1/Ce (L/mg)
0.14
0.12
0.10
0.08
0.06
0.04
0.02
0.00
0.00
0.05
0.10
0.15

Fig. 9.

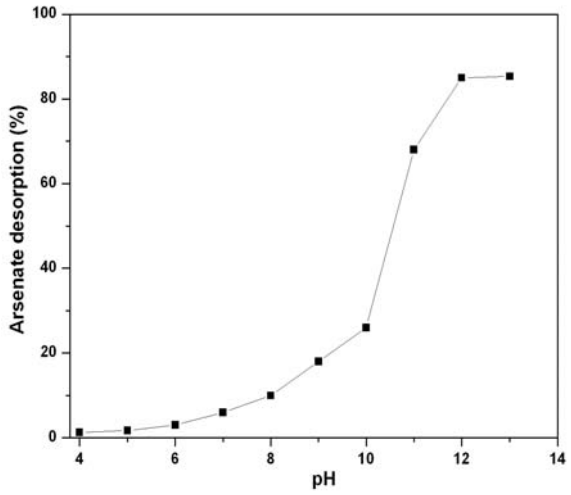
Arsenate desorption (%)
pH
100
80
60
40
20
0
4
6
8
10
12
14

Fig.10.

List of Table

Table 1. Pseudo-second-order kinetics constants and related regression coefficients

Table 1.

Initial solution pH	q_e (mg g^{-1})	K_2 (g mg^{-1} min^{-1})	R^2
5	52.604	6.234 x 10^{-3}	0.998
7	46.620	0.420 x 10^{-3}	0.999
9	34.106	1.395 x 10^{-3}	0.994